The Journal *of* Immunology

C2 Domains of Munc13-4 Are Crucial for Ca $^{2+}$ -Dependent Degranulation and Cytotoxicity in NK Cells

Na-Ryum Bin, Ke Ma, Chi-Wei Tien, Siyan Wang, Dan Zhu, Seungmee Park, Ekaterina Turlova, Kyoko Sugita, Ryutaro Shirakawa, Peter van der Sluijs, Hisanori Horiuchi, Hong-Shuo Sun, Philippe P. Monnier, Herbert Y. Gaisano and Shuzo Sugita

---

Supplementary Material	http://www.jimmunol.org/content/suppl/2018/06/07/jimmunol.1800426.DCSupplemental
References	This article **cites 60 articles**, 29 of which you can access for free at: http://www.jimmunol.org/content/201/2/700.full#ref-list-1

Why *The JI*? Submit online.

- **Rapid Reviews! 30 days*** from submission to initial decision

- **No Triage!** Every submission reviewed by practicing scientists

- **Fast Publication!** 4 weeks from acceptance to publication

*average

Subscription	Information about subscribing to *The Journal of Immunology* is online at: http://jimmunol.org/subscription
Permissions	Submit copyright permission requests at: http://www.aai.org/About/Publications/JI/copyright.html
Email Alerts	Receive free email-alerts when new articles cite this article. Sign up at: http://jimmunol.org/alerts

C2 Domains of Munc13-4 Are Crucial for Ca²⁺-Dependent Degranulation and Cytotoxicity in NK Cells

Na-Ryum Bin,*,† Ke Ma,*,† Chi-Wei Tien,*,† Siyan Wang,*,† Dan Zhu,†,‡
Seungmee Park,*,† Ekaterina Turlova,†,§ Kyoko Sugita,¶ Ryutaro Shirakawa,‖
Peter van der Sluijs,#,1 Hisanori Horiuchi,‖ Hong-Shuo Sun,†,§ Philippe P. Monnier,†,¶
Herbert Y. Gaisano,†,‡ and Shuzo Sugita*,†

In the immune system, degranulation/exocytosis from lymphocytes is crucial for life through facilitating eradication of infected and malignant cells. Dysfunction of the NK cell exocytosis process has been implicated with devastating immune diseases, such as familial hemophagocytic lymphohistiocytosis, yet the underlying molecular mechanisms of such processes have remained elusive. In particular, although the lytic granule exocytosis from NK cells is strictly Ca²⁺-dependent, the molecular identity of the Ca²⁺ sensor has yet to be identified. In this article, we show multiple lines of evidence in which point mutations in aspartic acid residues in both C2 domains of human Munc13-4, whose mutation underlies familial hemophagocytic lymphohistiocytosis type 3, diminished exocytosis with dramatically altered Ca²⁺ sensitivity in both mouse primary NK cells as well as rat mast cell lines. Furthermore, these mutations within the C2 domains severely impaired NK cell cytotoxicity against malignant cells. Total internal reflection fluorescence microscopy analysis revealed that the mutations strikingly altered Ca²⁺ dependence of fusion pore opening of each single granule and frequency of fusion events. Our results demonstrate that both C2 domains of Munc13-4 play critical roles in Ca²⁺-dependent exocytosis and cytotoxicity by regulating single-granule membrane fusion dynamics in immune cells. *The Journal of Immunology*, 2018, 201: 700–713.

Exocytosis of secretory lysosomal granules from immune cells, such as mast cells, NK cells, and CTLs, plays a crucial role in protecting individuals from invading pathogens as well as eradicating infected and malignant cells. Understanding the molecular basis of lysosomal exocytosis is important because impairments in such processes have led to severe immune disorders. Recent studies have found that soluble *N*-ethylmaleimide–sensitive factor attachment protein receptor (SNARE) complex and its regulating proteins, such as Rab27A, Munc18-2, and Munc13-4, are critical for immune cell exocytosis (1–7). In particular, mutations in Munc13-4, Munc18-2, and syntaxin-11 are associated with a fatal immune disorder: familial hemophagocytic lymphohistiocytosis (FHL) type 3 (FHL3), 4, and 5 (5, 8–12). FHL is a heterogeneous, life-threatening, genetic-based autosomal recessive immune disease characterized by uncontrolled hyperinflammation by overactivation of macrophages and lymphocytes. The CTLs and NK cells isolated from FHL3, FHL type 4, and FHL type 5 patients exhibited impaired cytotoxic granule exocytosis. Griscelli syndrome type 2 has been implicated with mutations in Rab27A, a protein that interacts with Munc13-4 for tethering of lysosomal granules (13). Importantly, exocytosis of secretory lysosomal granules in immune cells is Ca²⁺ dependent; however, the critical Ca²⁺ sensor for exocytosis remains unknown. This is in contrast to the extensively studied and highly established role of synaptotagmin-1 as a Ca²⁺ sensor for fast synchronous neurotransmitter exocytosis in neurons (14, 15).

The Munc13 protein family, which consists of Munc13-1, -2, and -3 (16), plays an essential role in the priming of synaptic vesicles (17). Munc13-4 and brain-specific angiogenesis inhibitor 1–associated protein 3 (BAP3) are distantly related to the core Munc13 family (Supplemental Fig. 1A). Structurally, Munc13-4 and BAP3 differ from the cognate Munc13 proteins in lacking three domains: an N-terminal C2 domain, a calmodulin-binding domain, and a diacylglycerol-binding C1 domain. Yet, they share two Munc homology domains (MHDs) and two C2 domains. In Munc13-1, -2, and -3, four aspartic acid residues, which are necessary to support Ca²⁺-dependent phospholipid binding, are preserved only in the C2B domain, whereas the Ca²⁺ binding sequence in the C-terminal C2C domain is degenerated (18). By

contrast, the key aspartic acid residues are preserved in both C2 domains (C2A, C2B) of different Munc13-4 and BAP3 orthologs across various species, including *Caenorhabditis elegans* and *Drosophila* (Supplemental Fig. 1B, 1C). Importantly, each of the C2 domains of Munc13-4 was found to bind Ca^{2+} (19), which is also predicted by a homology model (Supplemental Fig. 1D, 1E). Ca^{2+} binding to both C2 domains of Munc13-4 and synaptotagmin-1 shows great similarities; given that synaptotagmin-1 is a key Ca^{2+} sensor in neuronal exocytosis (14), this raises the possibility that Munc13-4 might act as a key Ca^{2+} sensor in immune cell exocytosis. To investigate this, we employed two different immune model systems: mast cell lines and primary NK cells. In this study, using a high-titer lentivirus infection system, we examined the role of Munc13-4 by rescuing Munc13-4–deficient primary NK cells as well as mast cell lines with human Munc13-4 variants in which key aspartic acids in C2A and C2B domains were mutated.

Materials and Methods

General materials

Parental pLKO-neo plasmid for lentivirus-mediated knockdown (KD) was purchased from Sigma-Aldrich (Oakville, ON, Canada). pLVX-IRES-puro plasmid for lentivirus-mediated expression was purchased from Clontech Laboratories (Mountain View, CA). psPAX2 was purchased from Addgene (Cambridge, MA). Rabbit Ab against full-length Munc13-4 was generated as described (20). We obtained monoclonal Abs of Munc18-1 (clone 31) from BD Biosciences (Mississauga, ON, Canada), GAPDH (clone 6C5) from Millipore (Billerica, MA), rabbit polyclonal Abs against syntaxin-4 from Synaptic Systems (Göttingen, Germany), and syntaxin-3 and syntaxin-11 from Proteintech (Chicago, IL). Rabbit polyclonal anti–Munc18-2 Ab was a kind gift from Dr. V. Olkkonen (Minerva Institute, Helsinki, Finland).

Animal models

C57BL/6J-Unc13d^jinx mice (Mutant Mouse Resource and Research Centers: 016137) were purchased from the Mutant Mouse Regional Resource Center at University of California, Davis (21). Wild-type (WT) and Unc13d^jinx/jinx homozygous mice were generated by crossing heterozygous mice. We used animals between 2 and 3 mo of age exclusively for all experiments without preferences on sex. The WT and Unc13d^jinx/jinx homozygous mice were cohoused in the same vivarium that was maintained between 22 and 23°C with a 12-h light on/off cycle. Food and water were accessible ad libitum. All experiments were reviewed and approved by the animal care committee of the University Health Network in accordance with the Canadian Guidelines for Animal Care.

Generation of stable Munc13-4 KD RBL-2H3 cells

Twenty-one–nucleotide short hairpin RNA sequences targeting rat Munc13-4 (5′-GCACAGTTGAATGGTTTCACC-3′) were annealed and ligated to pLKO-neo vector digested with EcoRI/AgeI. The hexameric sequence of 5′-CTCGAG-3′ was used as a linker sequence. After DNA sequencing, the construct was transfected into HEK-293FT cells along with psPAX2 and pCMV-VSVG for lentivirus generation. Lentivirus was harvested 3 d later and then applied to RBL-2H3 cells (American Type Culture Collection, Manassas, VA) for 2 d. Successfully infected cells were selected with G418 (700 μg/ml).

Generation of Munc13-4 knockout RBL-2H3 cells

pX330-U6-chimeric_BB-CBh-hSpCas9 (pX330) plasmid was purchased from Addgene (22). From rat Munc13-4 genomic sequence, a 19-bp sequence of 5′-CTGCTGTGCTATCTGCAGG-3′ containing PstI restriction site in exon 3 was targeted. AGG at the 3′ end served as the NGG protospacer adjacent motif sequence. The sequence was ligated to the pX330 plasmid using BbsI. The inserted sequence was verified by DNA sequencing. WT RBL-2H3 cells were cotransfected with pBabe-puro (1 μg) and pX330 containing Munc13-4 targeted sequence (10 μg) using electroporation (250 V, 975 μF, Gene Pulser; Bio-Rad, Hercules, CA) and maintained in growth medium containing 2.5 μg/ml puromycin (Bioshop, Burlington, ON, Canada) for 2 d. Using serial dilution, growing colonies were diluted, and single colonies were plated in 96-well plates. A knockout (KO) colony, no. 11-7, was then transferred to a 10-cm dish, and protein expression of Munc13-4 was confirmed by Western blotting.

Generation of stable Munc13-4–rescued RBL-2H3 cells

Expression plasmids were created by modifying the parental pLVX-IRES-puro. First, the puromycin resistance gene was replaced by a blasticidin resistance gene, creating pLVX-IRES-blast. Then, emerald GFP (EmGFP; Clontech Laboratories) was subcloned into BamHI site, generating pLVX-EmGFP-IRES-blast. CMV promoter was replaced with ubiquitin C promoter from pUB-GFP (23) using the ClaI/EcoRI site. cDNA of human Munc13-4 was mutated during site-directed mutagenesis to yield single (D127N, D133N, D941N, D947N), double (D127N/D133N, D941N/D947N), and quadruple (D127N/D133N/D941N/D947N) mutants. After DNA sequencing, WT and mutants were ligated to pLVX-UBC-IB-EmGFP with EcoRI/XbaI. These constructs were transfected into HEK-293FT cells along with psPAX2 and pCMV-VSVG for lentivirus production, which were applied to stable Munc13-4 KD or KO (no. 11-7) RBL-2H3 cells. Blasticidin (20 μg/ml) was applied to select successfully infected cells.

β-Hexosaminidase release assays from RBL-2H3 cells

β-Hexosaminidase release assays from RBL-2H3 cells were performed as described in (1, 6). For Ca^{2+} titration assay, amounts of $CaCl_2$ in PSS buffer were altered to achieve desired extracellular Ca^{2+} concentrations. For 0 mM Ca^{2+} condition, 0.1 mM EGTA was added to chelate any Ca^{2+} presence.

Cell preparation for confocal immunofluorescence microscopy

Confocal immunofluorescence microscopy of RBL-2H3 cells was performed as described in (1, 6). For stimulation, 2.5 μM ionomycin was added at either 2.2 or 10 mM extracellular Ca^{2+} for 1 h at 37°C before fixation.

Isolation and culture of primary NK cells from mouse spleen

MagCellect Mouse NK Cell Isolation Kit (catalog no. MAGM210) (R&D Systems, Minneapolis, MN) was used, following manufacturer's instructions for isolation. The isolated NK cells were cultured in complete media with RPMI 1640 (Sigma-Aldrich), supplemented with 10% FBS, penicillin (100 U/ml)/streptomycin (0.1 mg/ml), 2-ME (1.6 mM), and recombinant mouse IL-2 (1,000 U/ml; Thermo Fisher Scientific, Waltham, MA) in a 24-well plate. The plating density was 10,000 cells per well.

Lentivirus transduction and flow cytometry of NK cells

High-titer lentivirus was generated as described in (24). After harvesting supernatants, lentivirus was concentrated by centrifugation at 48000 × g for 2 h with 20% sucrose + 1 mM EDTA solution. The pellet was then resuspended in PBS + 1 mM EDTA, and the virus was stored at −80°C until use.

On day in vitro (DIV) 2, NK cells were transduced with a virus expressing EmGFP, Munc13-4 WT, or mutants fused with EmGFP, and the NK cells were used for experiments on DIV7.

The purity of the NK cells was assessed by flow cytometry analysis. Briefly, the cells were harvested and stained on ice for 30 min using PE-Cy7–conjugated anti-mouse NK1.1 Ab (clone PK136; BioLegend, San Diego, CA). After washing with complete media twice, the cells were subjected to flow cytometry (BD FACSCalibur; BD Biosciences). Live cells were gated by their size and granularity based on forward-scattered light and side-scattered light parameters. The purity of the NK cells was analyzed by PE-Cy7, and the infection of the lentivirus was analyzed by FITC signals in comparison with the unstained and uninfected NK cells.

CD107a degranulation assay

CD107a degranulation assay on the NK cells was followed as described in (25). Briefly, on DIV7, degranulation from the NK cells was stimulated with 2.5 μM ionomycin + 0.1 μM PMA. The cells were then stained with PE-Cy7–conjugated anti-mouse NK1.1 Ab. The flow cytometry analysis was performed on double-gated NK cells based on NK1.1, forward light scatter, and side scatter parameters. For the rescued NK cells, GFP+ and NK1.1+ NK cells were gated. Within this population, the NK cells that expressed higher intensity of cell surface CD107a than the unstimulated cells were considered to be degranulated, and their percentage among the total NK cells was calculated.

For CD107a degranulation assays in different Ca^{2+} concentrations, we replaced complete media (containing 0.4 mM Ca^{2+}) with the following media: complete media + 1 mM EDTA for 0 mM Ca^{2+}, complete media + 1.8 mM $CaCl_2$ for 2.2 mM Ca^{2+}, and complete media + 9.6 mM $CaCl_2$ for 10 mM Ca^{2+}.

Calcein Blue AM–based cytotoxicity analysis of NK cells

Cytotoxicity assays were performed as described in (26). K562 cells (American Type Culture Collection) were used as target cells, and 15 μM Calcein Blue AM (Thermo Fisher Scientific) dye was loaded. NK cells (effector cells) of DIV7 were harvested and washed twice in complete medium. Effector and target cells were plated with E:T ratios from 50:1 to 0.5:1. For experiments using rescued NK cells as effector cells, E:T ratios of 50:1 and 12.5:1 were performed. Released Calcein Blue AM was measured using a CLARIOstar microplate spectrofluorometer (BMG Labtech, Ortenberg, Germany) with excitation at 360 nm and emission at 445 nm. Emission intensity of supernatant/emission intensity of maximum release by 2% Triton X-100–treatment × 100% was calculated to be the percentage of target cell lysis by the effector cells.

Total internal reflection fluorescence microscopy

RBL-2H3 cells were transfected with neuropeptide Y fused with mCherry (NPY-mCherry) using electroporation (250 V, 975 μF, Gene Pulser) 4 d prior to total internal reflection fluorescence microscopy (TIRFM). Two days later, the cells were plated on a glass coverslip (25-mm diameter; Thermo Fisher Scientific) in six-well plates. Two days after plating, TIRFM was performed. Total internal reflection fluorescence microscope setup was constructed based on the prismless and through-the-lens configuration (27). A field of view containing 5–10 cells was chosen. Images were acquired at 5 Hz with a 100-ms exposure time using Nikon NIS-Elements software (Nikon, Mississauga, ON, Canada). Thirty seconds after the start of image acquisition, 2.5 μM ionomycin was gently added to the cells. A total of 2.2 and 10 mM Ca^{2+} containing PSS + 0.1% BSA buffer was used as a bath. A total of 7 min was obtained per recording.

TIRFM analysis

TIRFM movies were analyzed using ImageJ (National Institutes of Health, Bethesda, MD). Images were loaded on ImageJ as an audio–video interleave file. Using the MultiDot function of ImageJ, every visibly docked vesicle before the stimulation was marked manually (on average, ~50–60 vesicles per cell). Then, each dot was transformed into a circle with a two-pixel radius. Manual adjustment of circle location was done to make sure that the vesicles were fully surrounded by a circle with a two-pixel radius. Mean intensity of the circle along each successive frame was quantified using the MultiMeasure function of ImageJ. Vesicles that were visible before stimulation but did not undergo abrupt brightening followed by decay were considered as docked but not fusing vesicles (Supplemental Fig. 4A). Number of nonfusing vesicles/total vesicles per cell × 100% was expressed as nonfusion granule percentage. Among the fused vesicles per cell, fluorescence intensity increase was calculated from (peak intensity after stimulation − baseline intensity)/baseline intensity × 100%. They were then expressed as a population histogram. For kinetics, the average time taken from the application of stimulation to the peak of fluorescence intensity was calculated.

Statistics

Throughout the experiments, all statistical analyses were performed using Origin 9 (OriginLab, Northampton, MA). All error bars represent SEM. For comparison of two groups, a two-tailed t test was performed. For a comparison of two groups or more, one-way ANOVA was performed.

Homology modeling

The homology model of human Munc13-4 C2A and C2B (National Center for Biotechnology Information Reference Sequence accession no. NM_199242.2, https://www.ncbi.nlm.nih.gov/nuccore/120432045) was constructed based on a template crystal structure of rat Munc13-1 C2B (Protein Data Bank: 3KWU, https://www.rcsb.org/structure/3kwu) (18) and rat synaptotagmin-1 C2B (Protein Data Bank: 1TJX, https://www.rcsb.org/structure/1TJX) (28). Sequences of human Munc13-4 C2A (aa 84–263) or C2B (aa 904–1047) were input into a SWISS-MODEL server along with template crystal structures (29–32). The predicted crystal structures of C2 domains of Munc13-4 were generated based on sequence homology and were visualized with Jmol software.

Results

Munc13-4 is essential for Ca^{2+}-dependent mast cell degranulation

To test the hypothesis that Munc13-4 is a potential Ca^{2+} sensor, we first generated stable Munc13-4 KD where Munc13-4 is strongly silenced in RBL-2H3 cells, an established model cell for immune cell exocytosis (Fig. 1) (1, 6, 33, 34). Levels of proteins crucial for immune cell exocytosis, such as various isoforms of Munc18 and syntaxin, remained unchanged despite a drastic loss of Munc13-4 (Fig. 1A, 1B). We then measured the secretion capability of control and Munc13-4 KD cells by triggering exocytosis using IgE and ionomycin (0.5, 2.5 μM) with and without PMA (Fig. 1C). PMA (0.1 μM), which activates the protein kinase C pathway and partially mimics the signaling cascades of FcεRI activation by IgE, is known to potentiate ionomycin-induced exocytosis in this cell type (35, 36). In all cases, we observed vast reductions of exocytosis from Munc13-4 KD cells, confirming an important function of Munc13-4 in mast cell exocytosis (Fig. 1C). To test the Ca^{2+} dependence of mast cell exocytosis, we measured exocytosis triggered with either IgE or ionomycin while titrating the extracellular Ca^{2+} from 0.05 to 30 mM (Fig. 1D, 1E). In both cases, the exocytosis of control cells peaked at 2.2 mM Ca^{2+}, although there were marked reductions of secretion beyond this physiological Ca^{2+} concentration. In contrast, Munc13-4 KD cells strongly suppressed exocytosis throughout the wide range of extracellular Ca^{2+} concentrations. Thus, Ca^{2+}-dependent exocytosis is severely lost in the absence of Munc13-4.

Aspartate mutations in C2 domains alter Ca^{2+} sensitivity of mast cell degranulation

To further investigate the function of Munc13-4 as a Ca^{2+} sensor in immune cell exocytosis, we rescued the KD cells by stably expressing EmGFP-fused human Munc13-4 proteins, in which the conserved aspartic acid residues in the C2 domains are mutated to asparagine. The mutations in these residues were reported to exhibit almost complete abolishment of Ca^{2+} binding properties of the recombinant Munc13-4 protein (19). Specifically, we mutated two aspartic acid residues in either C2A (D127N/D133N) or C2B (D941N/D947N) as well as a combination of both (the quadruple mutant, D127N/D133N/D941N/D947N) (Fig. 2A). The immunoblot analysis revealed double and quadruple mutants are expressed at a level comparable to the WT (Fig. 2B). We found that human WT Munc13-4 completely restored the defective exocytosis of Munc13-4 KD cells to that of control RBL-2H3 cells (Fig. 2C), which illustrates that the reduction of exocytosis seen from Munc13-4 KD was not due to any off-target effects of short hairpin RNA–mediated KD. However, double mutants of either the C2A or C2B domain failed to exhibit rescue ability toward IgE-dependent and ionomycin-induced secretion. Interestingly, they did show some levels of rescue in secretion upon the degranulation induced by ionomycin and PMA, with the C2A double mutant exhibiting better rescue ability than the C2B double mutant. A very slim margin of rescue in degranulation was observed from the quadruple mutant–rescued cells even with the strongest stimulation (Fig. 2C).

To assess the effects of the C2 domain mutations on Ca^{2+} dependency in exocytosis, we stimulated the cells with ionomycin (0.5 or 2.5 μM) and titrated the extracellular Ca^{2+} concentrations either with or without the presence of PMA (Fig. 2D–G). Similar to control cells, we observed the bell-shaped response of exocytosis from the WT Munc13-4–EmGFP-rescued cells. Strikingly, double and quadruple mutants of the C2 domains exhibited markedly altered Ca^{2+} sensitivity of exocytosis. They showed some level of secretion at 2.2 mM Ca^{2+}, and they invariably displayed a trend of positive increases in exocytosis at higher Ca^{2+} concentrations. The KD cells rescued by EmGFP not only exhibited almost complete abolishment of exocytosis even at 10 mM Ca^{2+} but also did not result in any Ca^{2+} dependency. Additionally, finer titration (between 0.1 and 2.2 mM) of extracellular Ca^{2+} revealed a similarly right-shifted Ca^{2+} sensitivity in
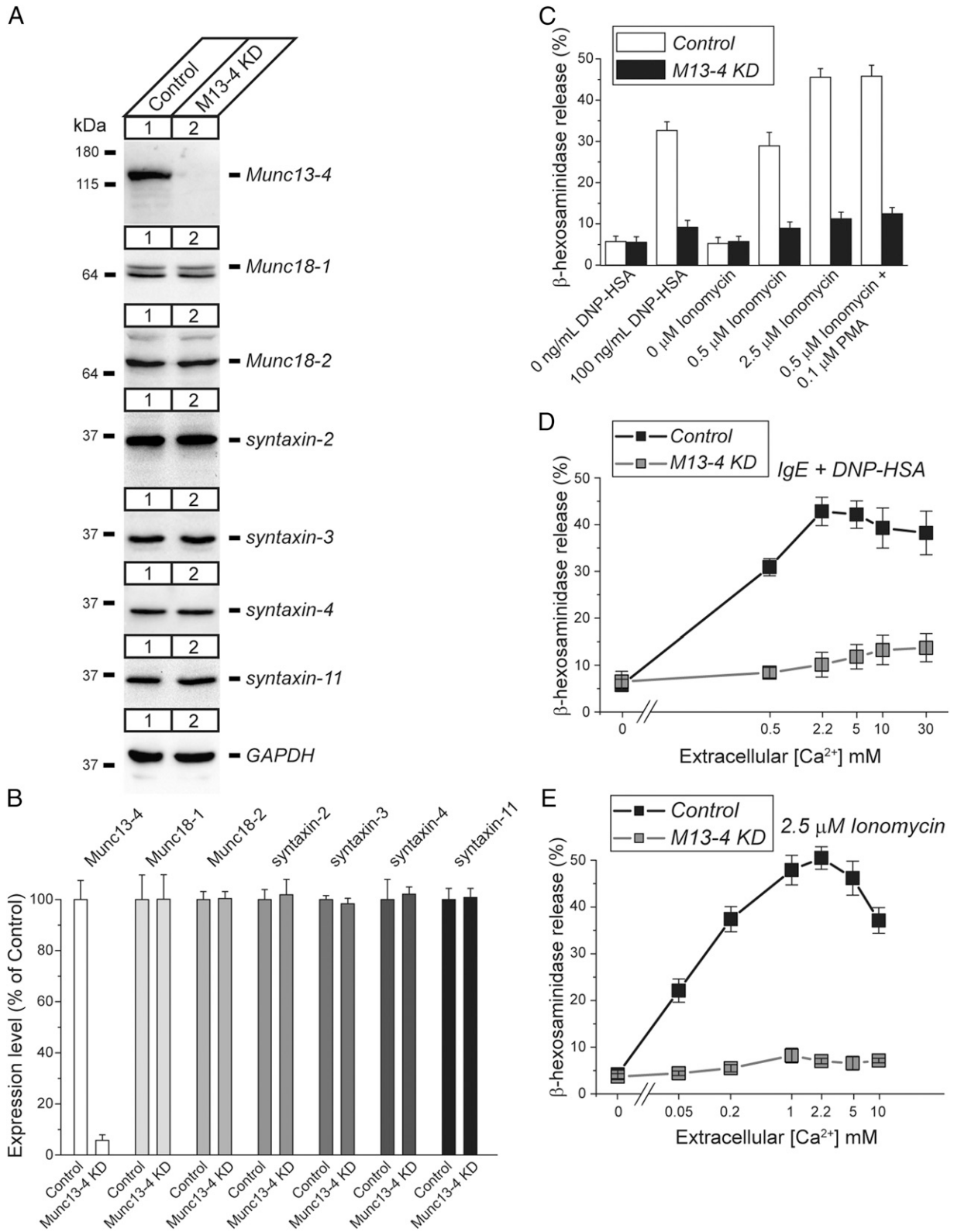
FIGURE 1. Loss of Ca^{2+} dependency in exocytosis from Munc13-4 KD mast cells. (**A**) Immunoblotting analysis of various secretory proteins in control and Munc13-4 KD cells. (**B**) Quantification of protein expression levels in Munc13-4 KD cells normalized to control cells. Error bars indicate SEM ($n = 6$). (**C**) β-Hexosaminidase release from the control and Munc13-4 KD cells was triggered by 1 h of incubation with indicated stimulations at 2.2 mM extracellular Ca^{2+}. Error bars indicate SEM ($n = 6$). (**D** and **E**) Titration of extracellular Ca^{2+} of control and Munc13-4 KD cells when stimulated with IgE + DNP–human serum albumin or ionomycin. Error bars indicate SEM ($n = 6$).

these mutants (Fig. 2H, 2I), which suggests that both domains need to be functional for Munc13-4 to be an effective Ca^{2+} sensor for exocytosis.

Next, we sought to identify the critical aspartic acid residue in the C2 domain that is involved in Ca^{2+} sensing of exocytosis. For this purpose, we rescued the KD cells with Munc13-4, which has a

FIGURE 2. Ca^{2+} sensitivity of mast cell exocytosis is strikingly altered upon mutations in C2 domains of Munc13-4. (**A**) Schematic diagram showing locations of point mutations i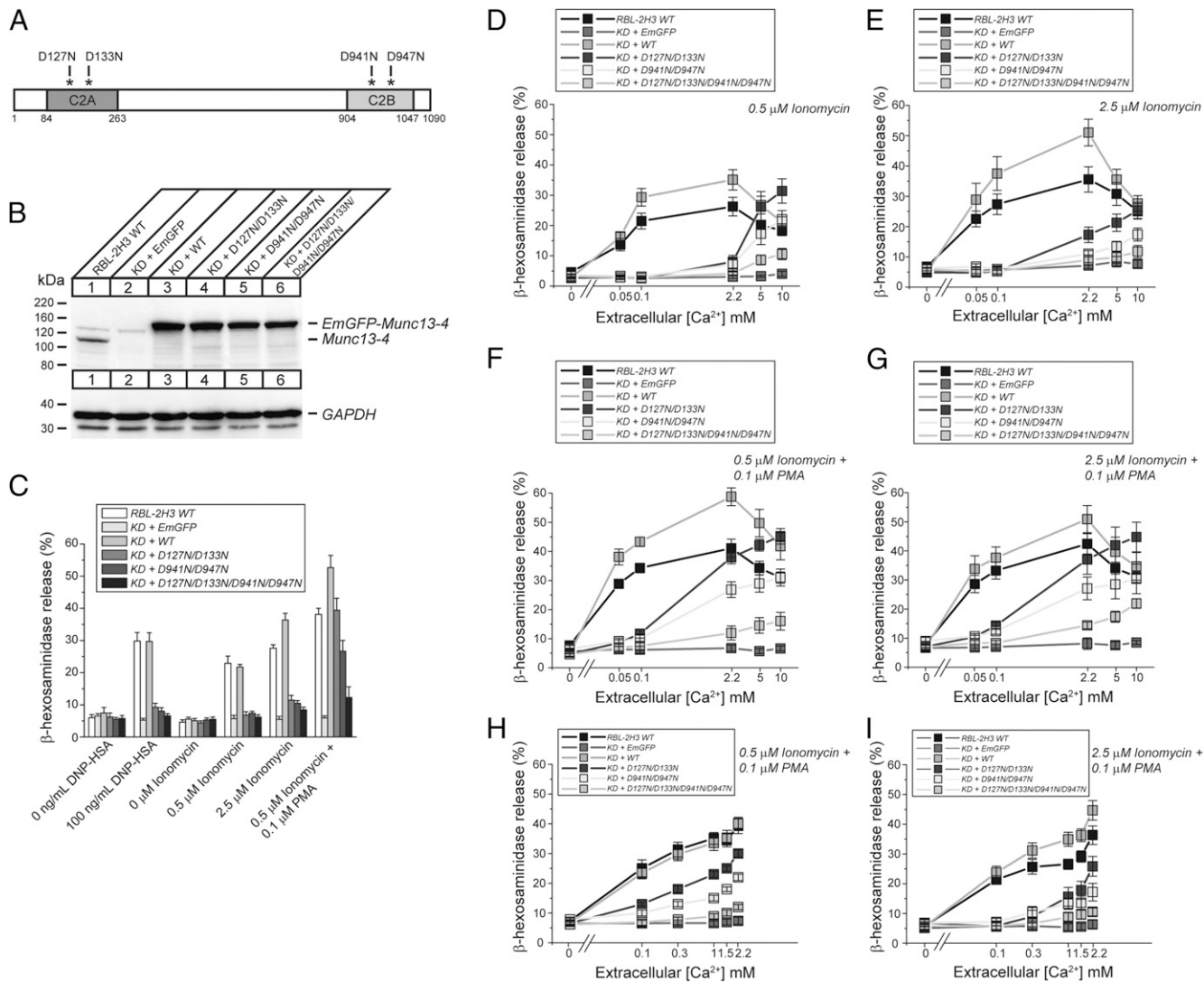n C2 domains of human Munc13-4. (**B**) Immunoblotting analysis of Munc13-4 KD cells rescued with EmGFP-fused WT, C2A, or C2B domain double mutants or quadruple mutant. (**C**) β-Hexosaminidase release from the Munc13-4 KD cells rescued with double and quadruple mutants in C2 domains was triggered by 1 h of incubation with indicated stimulations at 2.2 mM Ca^{2+}. Error bars indicate SEM ($n = 6$). (**D–G**) Titration of extracellular Ca^{2+} from 0.05 to 10 mM of Munc13-4 KD cells rescued with double and quadruple mutants in C2 domains triggered by (D) 0.5 μM ionomycin, (E) 2.5 μM ionomycin, (F) 0.5 μM ionomycin + 0.1 μM PMA, and (G) 2.5 μM ionomycin + 0.1 μM PMA. Error bars indicate SEM ($n = 6$). (**H** and **I**) Titration of extracellular Ca^{2+} between 0.1 mM and 2.2 mM for Munc13-4 KD cells rescued with double and quadruple mutants in C2 domains triggered by (H) 0.5 μM ionomycin + 0.1 μM PMA and (I) 2.5 μM ionomycin + 0.1 μM PMA. Error bars indicate SEM ($n = 6$).

single mutation in either the C2A or the C2B domain (Supplemental Fig. 2). Upon testing their rescue ability, we saw that the single-point mutants seem to support exocytosis better than their respective double mutants at 2.2 mM (Supplemental Fig. 2B). Nevertheless, Ca^{2+} sensitivities of all single mutants are still strikingly altered (Supplemental Fig. 2C–F). These results suggest that Munc13-4 plays a dual role in exocytosis: priming and sensing Ca^{2+}. As a whole protein, Munc13-4 is essential for exocytosis regardless of the extracellular Ca^{2+}, confirming that this protein is essential for priming exocytosis (5). In contrast, specific mutations in the C2 domains seem to selectively impair the functions of this protein as a Ca^{2+} sensor for exocytosis.

Mutations in C2 domains impair degranulation and its Ca^{2+} sensitivity in NK cells

Next, we sought to investigate whether our findings in mast cell degranulation are also true for lytic granule exocytosis in primary NK cells. As low or absent NK cell exocytosis from patients is one

of the diagnostic parameters of FHL3 disease (37), assessing the effect of C2 domain mutations in NK cell exocytosis would provide further insights toward the nature of FHL3. To address this issue, we employed NK cells isolated from Munc13-4 KO mice and their littermates as controls. First, we purified NK cells from Munc13-4 KO and control mice using a commercial kit, which is based on negative selection to avoid activation of NK cells. This kit offered 70–80% purity, which we were able to achieve. We confirmed >70% purity via anti-NK1.1 Ab staining. NK1.1, also known as KLRB1, is an Ag expressed on the surface of NK cells that has long been used as a marker of murine NK cells from the C57BL/6 mouse strain (38). We then measured the level of exocytosis in the NK1.1$^+$ NK cells by stimulating and measuring surface expression of CD107a, a cytotoxic granule marker, using FACS. We confirmed that the NK cells isolated from Munc13-4 KO mice exhibit diminished exocytosis as previously reported (Supplemental Fig. 3A–C) (21), which is also consistent with the phenotype of NK cells isolated from FHL3 patients (5).

FIGURE 3. Rescue of defective degranulation of Munc13-4 KO NK cells with lentivirus expressing WT Munc13-4. Degranulation assays of Munc13-4 KO primary NK cells that were transduced with lentivirus expressing EmGFP or WT Munc13-4–EmGFP. Degranulation was triggered with 2.5 μM ionomycin + 0.1 μM PMA for 6 h, and surface expression of CD107a was measured by FACS analysis. (**A**) Contour plots of FACS analysis illustrating induction of CD107a surface expression in NK1.1+ primary NK cells that were transduced with EmGFP or WT Munc13-4 in unstimulated (top) and stimulated (bottom) condition. (**B**) Overlay of CD107a histograms in unstimulated (black) and stimulated (gray) NK cells. (**C**) A bar graph showing CD107a degranulation from EmGFP-rescued (white) and WT Munc13-4–rescued (black) KO NK cells. Error bars indicate SEM ($n = 4$).
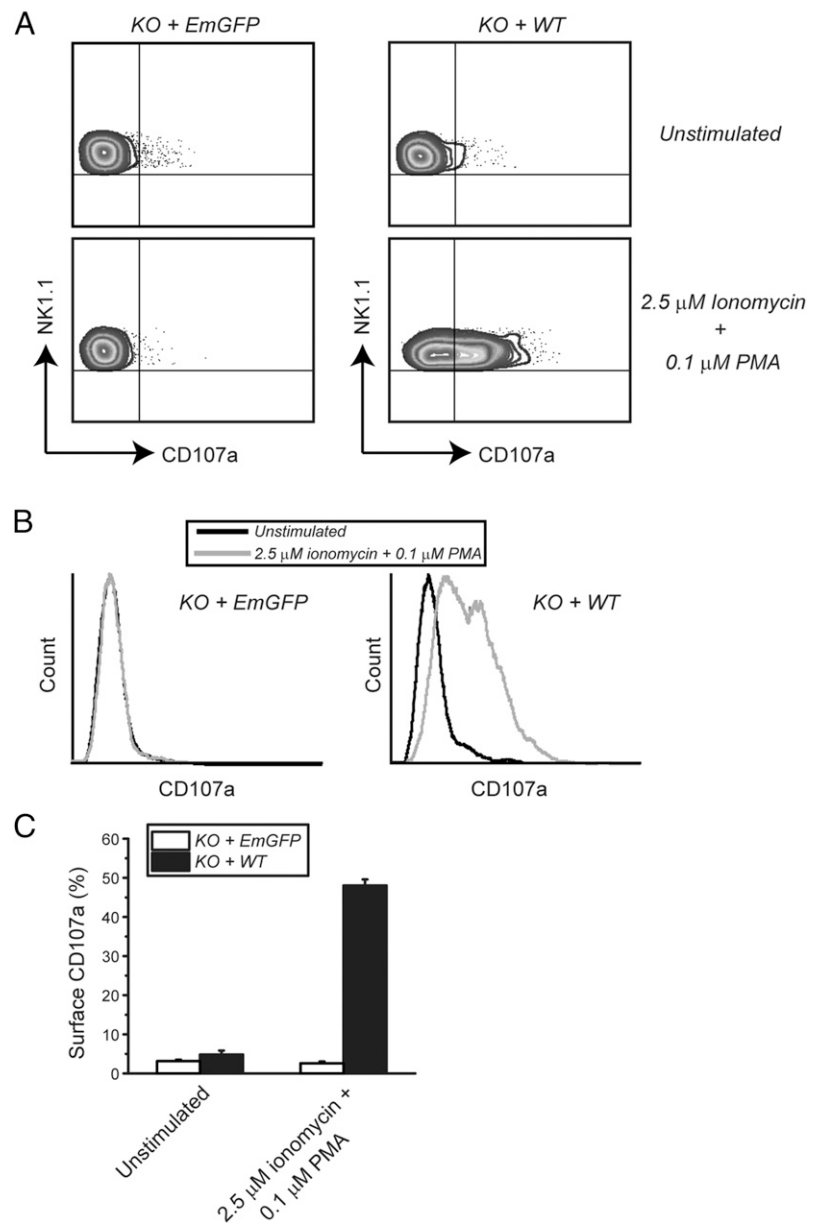
We then examined whether the diminished exocytosis in KO cells can be restored by expressing human Munc13-4 protein. Protein expression was driven by ubiquitin ligase C promoter, which was effective in the primary NK cells (39). After our infection of the NK cells with EmGFP or WT Munc13-4–EmGFP-expressing lentivirus, we found that >60% cells exhibited EmGFP signal within 3 d (Supplemental Fig. 3D). Five days postinfection, we examined the ability of the expressed proteins to rescue exocytosis using FACS assays. We found that transduction with human WT Munc13-4–EmGFP, but not EmGFP alone, was able to fully restore the exocytosis in KO NK cells (Fig. 3).

Using this rescue system, we examined whether single, double, or quadruple mutations in Munc13-4 C2 domains affect lytic granule exocytosis as well as its Ca^{2+} sensitivity (Figs. 4, 5). To examine the Ca^{2+} sensitivity, we triggered secretion under two different concentrations of extracellular Ca^{2+} (2.2 and 10 mM). First, we confirmed that the Ca^{2+} sensitivity was restored by the re-expression of WT Munc13-4 (Figs. 4, 5, Supplemental Fig. 3F–H). Upon testing the mutants, however, we found severe impairment of CD107a exocytosis compared with the WT. In addition,

we observed an increase of CD107a exocytosis from the C2 domain mutant-rescued NK cells when 10 mM Ca^{2+} was used, whereas such a higher concentration of Ca^{2+} decreased exocytosis from WT-rescued KO NK cells (Figs. 4, 5). Thus, we conclude that C2 domain mutations affect both efficacy and Ca^{2+} sensitivity of degranulation from the NK cells.

Aspartate mutations in Munc13-4 C2 domains impair cytotoxicity of NK cells against K562 cells

We also explored the functional outcomes of C2 domain mutations in Munc13-4 on the NK cells. Ca^{2+}-dependent exocytosis of perforin and granzymes from lytic granules of NK cells is believed to be the key mechanism of the NK cell–mediated cytotoxicity. We verified that WT NK cells exhibit robust cytotoxicity against human leukemic cell line K562 cells in a dose-dependent manner (26). However, Munc13-4 KO NK cells almost completely lose cytotoxicity even at a 50:1 ratio, confirming the crucial role of Munc13-4 protein in the NK cell cytotoxicity (21) (Fig. 6A). Next, we examined the cytotoxicity of NK cells rescued with human WT or C2 domain mutants of Munc13-4. All WT and mutant-rescued
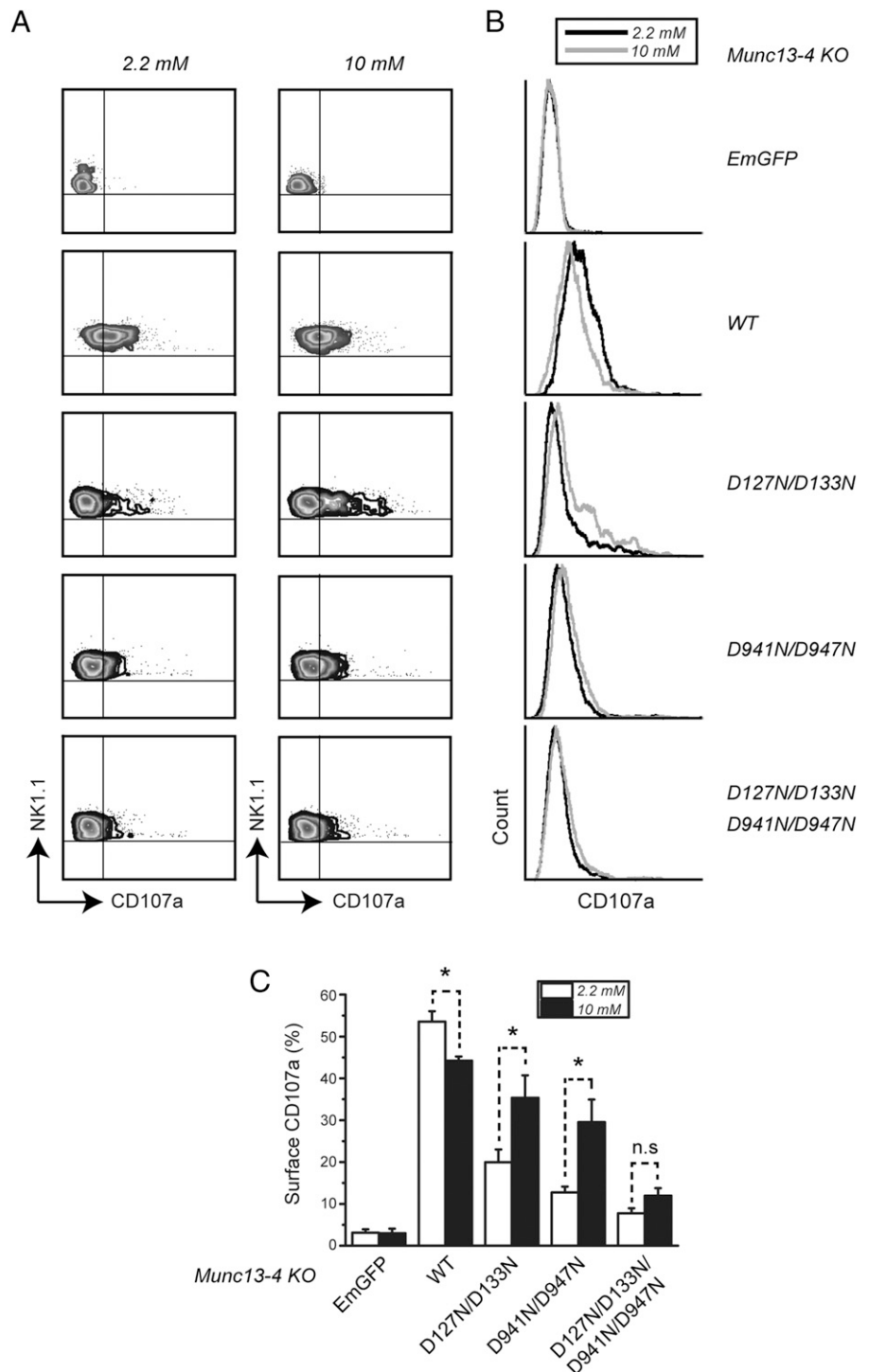
FIGURE 4. Double and quadruple mutations in the C2 domains of Munc13-4 alters Ca^{2+} sensitivity of degranulation from NK cells. Degranulation assays of Munc13-4 KO primary NK cells that were transduced with lentivirus expressing EmGFP alone, WT, C2 domain double, or quadruple mutant Munc13-4–EmGFP. Degranulation was triggered with 2.5 μM ionomycin + 0.1 μM PMA for 6 h and surface expression of CD107a was measured by FACS analysis. (**A**) Contour plots of FACS analysis illustrating induction of CD107a surface expression in NK1.1$^+$ primary NK cells in 2.2 mM (left) and 10 mM (right) extracellular Ca^{2+}. (**B**) Overlay of CD107a histograms in 2.2 mM (black) and 10 mM (gray) NK cells. (**C**) A bar graph showing CD107a degranulation from rescued NK cells in 2.2 mM (white) and 10 mM (black). Error bars indicate SEM ($n = 4$). *$p < 0.05$.

NK cells exhibited dose-dependent cytotoxicity of the K562 target cells at E:T ratios of 50 and 12.5:1 (Fig. 6B). However, although the WT re-expression clearly rescued defective cytotoxicity of KO NK cells, all mutants exhibited impairments in lysis of the target cells. Among the mutants, D133N-expressed NK cells showed better cytotoxicity than D947N, which is consistent with our findings that the mutants in the C2A domain of Munc13-4 showed better rescue ability than C2B domain mutants (Figs. 2, 4, 5, Supplemental Fig. 2). Double and quadruple mutants exhibited only a small margin of rescue in cytotoxicity, even at 50:1 ratio. Therefore, the C2 domains of Munc13-4 are crucial for exocytosis of lytic granules and thus critical for NK cytotoxicity against malignant cells.

Mutations in C2 domains do not alter subcellular localization of Munc13-4 nor impair its translocation upon stimulation

What underlies the impaired Ca^{2+}-dependent exocytosis in mutant Munc13-4? As a potential mechanism, we examined whether the localization or translocation of this protein in response to Ca^{2+} is altered (Fig. 7). Munc13-4 is known to localize at lysosomal granules by interacting with Rab27a found on the granules (7, 20). In the course of this study, CRISPR/Cas9-mediated genome editing was developed (40, 41). Based on this, we generated Munc13-4 KO RBL-2H3 cells (see *Materials and Methods*). We then expressed Munc13-4 EmGFP variants using high-titer lentivirus in the Munc13-4 KO RBL-2H3 cells, and EmGFP
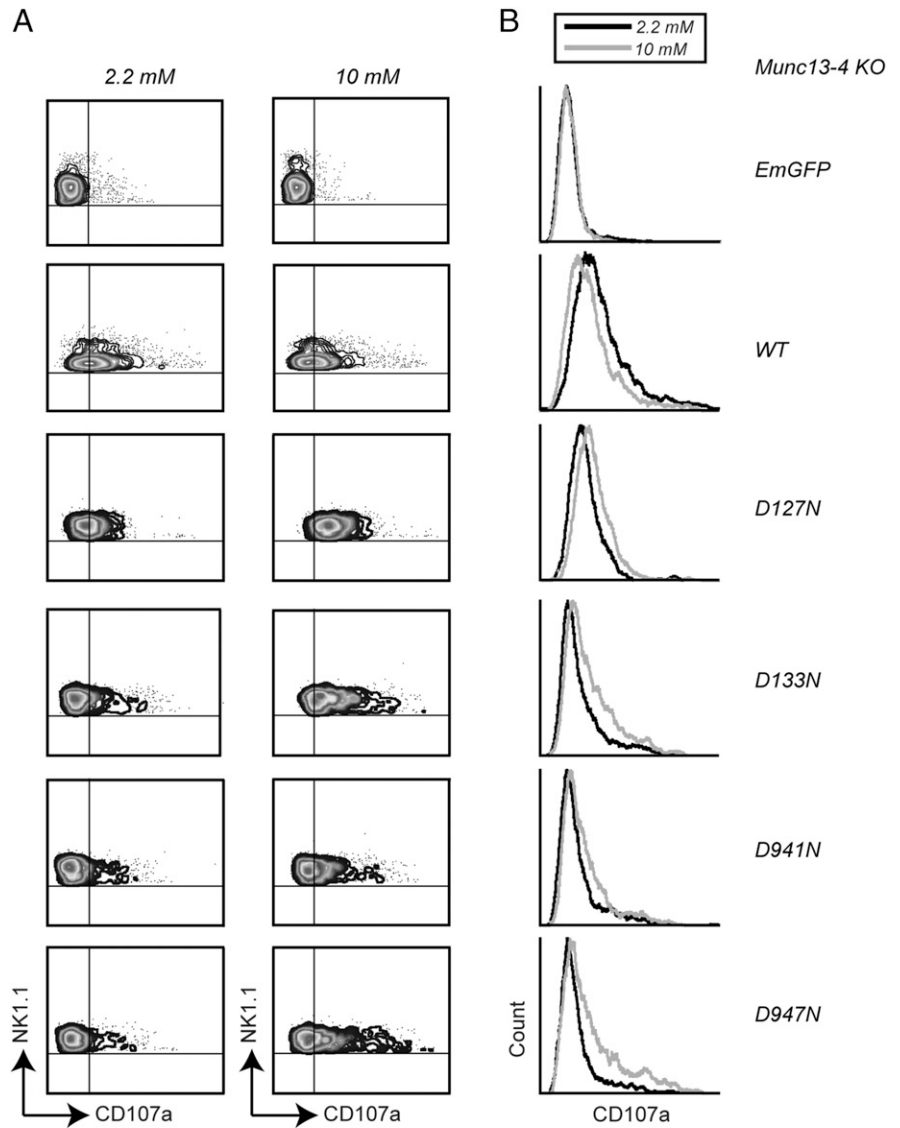
FIGURE 5. Single-point mutations in the C2 domains of Munc13-4 alter Ca^{2+} sensitivity of degranulation from NK cells. Degranulation assays of Munc13-4 KO primary NK cells that were transduced with lentivirus expressing EmGFP alone, WT, or C2 domain single-mutant Munc13-4 EmGFP. Degranulation was triggered with 2.5 μM ionomycin + 0.1 μM PMA for 6 h and surface expression of CD107a was measured by FACS analysis. (**A**) Contour plots of FACS analysis illustrating induction of CD107a surface expression in NK1.1[+] primary NK cells in 2.2 mM (left) and 10 mM (right) extracellular Ca^{2+}. (**B**) Overlay of CD107a histograms in 2.2 mM (black) and 10 mM (gray) NK cells. (**C**) A bar graph showing CD107a degranulation from rescued NK cells in 2.2 mM (white) and 10 mM (black). Error bars indicate SEM (n = 4). *$p < 0.05$.

fluorescence signal was visualized under confocal microscopy (Fig. 7). We found that EmGFP-fused Munc13-4 WT and mutants exhibit similar punctate signals, consistent with Munc13-4 being associated with secretory lysosomes (7, 20, 42). After the stimulation with 2.5 μM ionomycin in the presence of 2.2 or 10 mM extracellular Ca^{2+} concentration, Munc13-4 WT or mutants were found to be translocated to the plasma membrane. This is in agreement with a finding that Munc13-4 is recruited to the plasma membrane following stimulation in human neutrophils (43). We found that the translocation to the plasma membrane was similarly observed in all cases. Thus, the defective Ca^{2+} sensitivity of immune cell exocytosis seen from the mutants does not seem to be explained by their localization.
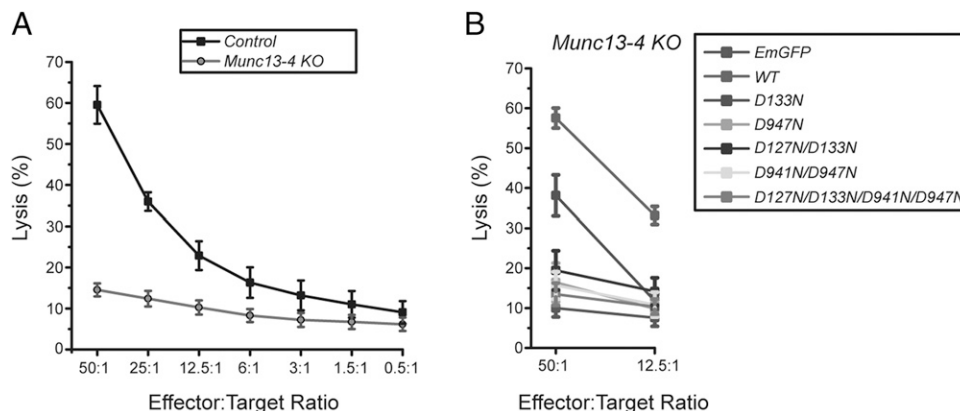
FIGURE 6. Mutations in C2 domains of Munc13-4 drastically reduces cytotoxicity of NK cells. (**A**) Control and Munc13-4 KO NK cells (effector cells) were incubated with Calcein Blue AM–loaded K562 cells (target cells) at indicated E:T ratios for 4 h, and the amount of Calcein Blue AM was measured. Percentage of lysis was calculated by dividing the amount of Calcein Blue AM by the total amounts (2% Triton X-100) × 100%. Error bars indicate SEM ($n = 12$). (**B**) Cytotoxicity assay of Munc13-4 KO NK cells that are transduced with lentivirus expressing EmGFP, WT, or indicated C2 domain mutants. E:T ratios were 50:1 and 12.5:1. Error bars indicate SEM ($n = 9$).

TIRFM analysis reveals crucial role of Munc13-4 in single-granule fusion dynamics in a Ca²⁺-dependent manner

Next, we asked whether the altered Ca²⁺ sensitivity is due to changes in the frequency of the vesicular fusion events and/or whether it is due to different sizes of fusion pore formation of single-vesicle fusion at different Ca²⁺ concentrations. For this purpose, we transfected mast cells with cDNA of a cargo molecule (NPY-mCherry) and examined their release using TIRFM (Fig. 8). Under an evanescent field, we observed a comparable number of granules in control and Munc13-4 KD cells, suggesting that the NPY-mCherry is similarly expressed in the absence of Munc13-4 (Fig. 8A).

To reveal the Ca²⁺ dependence of a single-vesicle fusion, we used two different extracellular Ca²⁺ concentrations (2.2 and 10 mM) and stimulated the exocytosis with 2.5 μM ionomycin and monitored release of NPY-mCherry. A granule fusion event was evident when a rapid increase of fluorescence intensity after the stimulation was followed by a steady decay (Fig. 8B). Additionally, there were granules that appeared in the evanescent field but failed to exhibit a rapid increase of fluorescence signal and a steady decay afterward (Supplemental Fig. 4A). These granules were classified as nonfusion granules. This observation is consistent with a previous report on the analysis of nonfusing vesicles from neuroendocrine cells assessed under TIRFM (44). In control cells at 2.2 mM Ca²⁺, the release of NPY-mCherry caused a rapid and large increase in the fluorescence signal, which then quickly decayed (Fig. 8B). Most granules seemingly underwent exocytotic fusion in the control cells, with nonfusion granules consisting of only 9.7% of the total granule population (Fig. 8C). However, upon triggering exocytosis at 10 mM, the control cells exhibited an increase of nonfusion events of granules, indicating the frequency of fusion events was reduced at this high Ca²⁺ (Fig. 8C). Unexpectedly, the kinetics and amplitudes of NPY-mCherry release were also severely compromised (Fig. 8D, 8E). Namely, time to reach the peak of the fluorescence intensity was substantially delayed at 10 mM compared with 2.2 mM Ca²⁺ (Fig. 8D). In addition, increase of fluorescence intensity amplitude from a single-granule fusion event was dramatically lower at 10 mM Ca²⁺ (Fig. 8E). In contrast, Munc13-4 KD cells had exhibited substantially augmented population of nonfusion granules at 2.2 mM Ca²⁺ (Fig. 8C). Moreover, among the fused granules, the increase of fluorescence intensity amplitude was substantially lower than control cells (Fig. 8D, 8E).

Such phenotypes of single-granule fusion events from the KD cells remained similar at 10 mM Ca²⁺ (Fig. 8D, 8E). These results suggest important functions of Munc13-4 in single-granule fusion events of mast cells; it regulates not only the frequency of fusion events but also the kinetics and magnitudes of cargo release, presumably by regulating the opening and size of fusion pore in a Ca²⁺-dependent manner.

Point mutants in C2 domains of Munc13-4 alters Ca²⁺ sensitivity of single-granule fusion dynamics

We next tested the effects of Ca²⁺ binding mutations in the C2 domains of Munc13-4 on single-granule fusion events. First, we observed that the re-expression of WT Munc13-4, but not EmGFP, was able to restore decreased frequency, altered kinetics, and amplitudes of fusion events of KD cells at 2.2 mM (Fig. 9A, 9C–E). Upon testing double mutants and quadruple C2 domain mutants, we found that the Ca²⁺ dependency of their frequency and opening of fusion pores in single-granule fusion events was significantly shifted (Fig. 9B–D, 9F). At 2.2 mM, all of the C2 domain mutants exhibited impaired single-granule fusions such that there were substantially increased nonfusion events, and the granules that were fused exhibited reduced amplitudes compared with the WT-rescued cells (Fig. 9C, 9F). Moreover, the average time taken to reach the peak of fluorescence intensity was significantly longer than the WT (Fig. 9D). However, these compromised fusion dynamics were invariably alleviated when it was triggered at 10 mM Ca²⁺. The percentage of nonfusion granules was significantly decreased compared with 2.2 mM. In addition, the amplitude and kinetics of the fusion events were both greater and faster at this elevated Ca²⁺ (Fig. 9B–D, 9F). This shifted Ca²⁺ sensitivity was recapitulated in cells rescued with single mutations of the C2 domains (Supplemental Fig. 4). In conclusion, mutations in the C2 domains of Munc13-4 alter two independent parameters of Ca²⁺-dependent vesicle fusion: 1) the size and kinetics of fusion pore opening in single vesicles and 2) the frequency of fusion events (Fig. 10).

Discussion

In this study, we showed that Ca²⁺ binding of both C2 domains in Munc13-4 is crucial for degranulation (Figs. 4, 5, Supplemental Fig. 3A–C, 3F–H) and cytotoxicity (Fig. 6) of NK cells as well as mast cells (Figs. 1, 2, Supplemental Fig. 2). Conservation of the key aspartic acid residues in both C2 domains (C2A, C2B) of
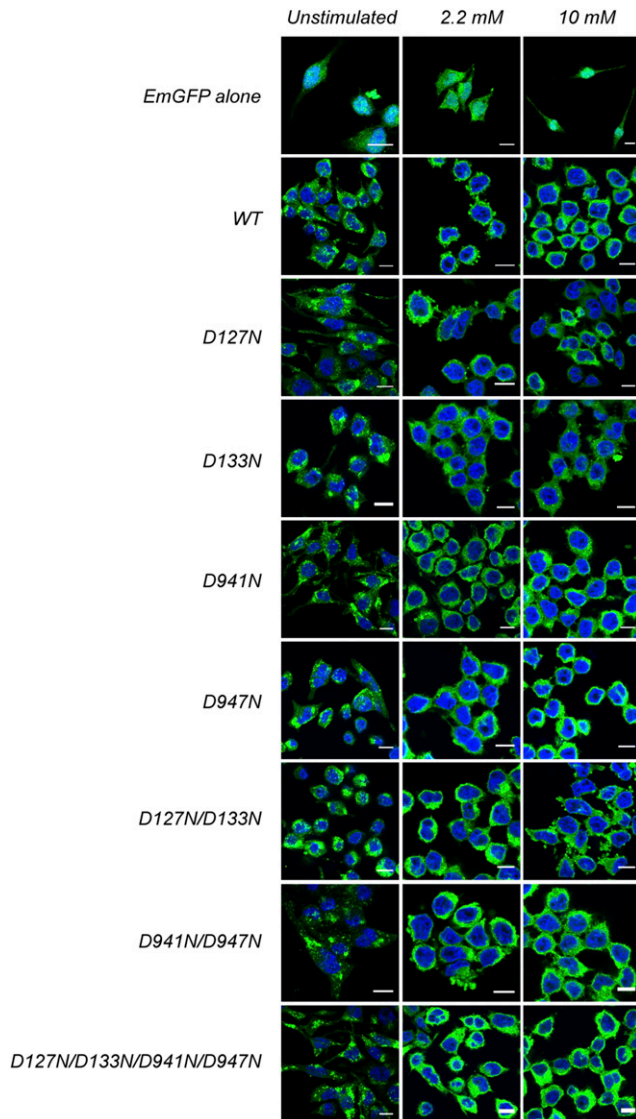
FIGURE 7. Translocation of Munc13-4 to the plasma membrane upon stimulation does not exhibit Ca^{2+} dependency. Munc13-4 KO RBL-2H3 cells expressing EmGFP alone, EmGFP-fused WT, or C2 domain mutants were stimulated with 2.5 μM ionomycin at 2.2 or 10 mM extracellular Ca^{2+} for 1 h. The cells were then fixed, counterstained with DAPI, and mounted. Images were acquired by confocal microscope. Scale bars, 10 μm.

Munc13-4 is more similar to synaptotagmin-1, a key Ca^{2+} sensor in neuronal exocytosis (14), rather than Munc13-1, -2, or -3, whose Ca^{2+} binding sequences in the C2C domain are degenerated (Supplemental Fig. 1) (18). Our data suggest that the Ca^{2+} binding property of the C2 domains of Munc13-4 are indeed crucial for determining the Ca^{2+} sensitivity of exocytosis from immune cells. This markedly altered Ca^{2+} sensitivity is similarly observed from the C2 domain mutants of synaptotagmin-1 (45), which may indicate conserved mechanisms of Ca^{2+} sensing exerted by the two proteins in different cell types (Fig. 10). Although our results suggest that Munc13-4 is the key Ca^{2+} sensor for exocytosis in immune cells, they do not exclude a possibility that the Ca^{2+}-sensing function of Munc13-4 is achieved via a collaborative function with synaptotagmin proteins (Fig. 10). Nevertheless, in the current state of knowledge, which synaptotagmin isoforms whose C2 domain mutations could affect Ca^{2+} sensitivity of exocytosis in immune cells have yet to be identified.

Previous work that assessed the function of the C2 domains of Munc13-4 were limited to the studies employing permeabilized RBL-2H3 cells, liposome fusion assays, and platelets. Using reconstitution assay, it was shown that baculovirus-purified recombinant Munc13-4, but not the C2 domain mutants, was able to restore Ca^{2+}-dependent granule exocytosis in permeabilized cells. Biochemically, Munc13-4 exhibited Ca^{2+}-stimulated SNARE complex and lipid interactions through the C2 domains (19). Another group demonstrated that Munc13-4 enhanced Ca^{2+}-dependent liposome fusions and that its absence resulted in a higher mobility of granules in platelets, suggesting a tethering role of Munc13-4 (46). However, whether the C2 domains are involved in the tethering function of Munc13-4 in platelets was not addressed. In addition, without rescue experiments, these previous studies could not delineate the functional role of the C2 domains on exocytosis from the intact cells. Our comprehensive rescue approaches and Ca^{2+} titrations in both mast cells and primary NK cells clearly reveal the crucial function of the C2 domains in Ca^{2+} sensitivity of exocytosis in intact immune cells. Therefore, to our knowledge, our present data are the first to demonstrate that the Ca^{2+} binding ability of both C2 domains of Munc13-4 is crucial for the Ca^{2+} sensing of exocytosis in live mast cells and the primary NK cells.

Despite clear evidence for the role of Munc13-4 in immune cell exocytosis, our results have several concerns that need to be discussed. The following criticisms can be postulated: 1) potential misfolding of mutant Munc13-4, 2) potential dysfunction of human Munc13-4 in rat RBL-2H3 mast cells and mouse NK cells because of cross-species, and 3) role of Munc13-4 in different configurations of lytic synapses between mast cells and NK cells. First, structural studies have revealed that mutating Ca^{2+} binding residues in the C2 domains of synaptotagmin-1 affects the Ca^{2+} binding affinity without changes in the overall structure of the C2 domains (14, 47). Our homology model suggests that the C2 domains of Munc13-4 exhibit a similar structure to those of synaptotagmin-1 (Supplemental Fig. 1D, 1E). Moreover, the fact that the C2 domain mutants, which are expressed (Fig. 2, Supplemental Fig. 2) and correctly localized as the WT (Fig. 7), are able to support exocytosis at higher Ca^{2+} concentrations indicates that the mutant proteins are functional, although they exhibit lower Ca^{2+} binding ability. Second, cross-species experiments are of a concern when the sequence homologies of the orthologs in different species are invariably low. Nonetheless, for the case of Munc13-4, the amino acid sequence identity between rat and mouse reaches 94% shared homology, whereas human and rat/mouse is 88% shared homology (determined by Basic Local Alignment Search Tool sequence alignment). Moreover, putative Ca^{2+} binding residues in the C2 domains of Munc13-4 are all conserved throughout different species (Supplemental Fig. 1A–C). Therefore, although there can be subtle differences of Munc13-4 in various species, the majority of its functions, especially the Ca^{2+} binding mechanism of the C2 domains, seems to be largely conserved between Munc13-4 orthologs. Last, although NK cells and mast cells are distinct in their modes of activation and target cells, the mechanism of regulated fusion of the lytic granules and secretory lysosomes share SNARE protein involvement (48, 49). More importantly, priming of vesicles in both cells requires Munc13-4 (50–52). Thus, although we cannot exclude a potential role of Munc13-4 in earlier stages, the function of Munc13-4 in Ca^{2+}-dependent degranulation (exocytosis) seems to be highly conserved in both NK cells and mast cells. Future studies investigating the differential role of Munc13-4 in distinct lytic synapses of two
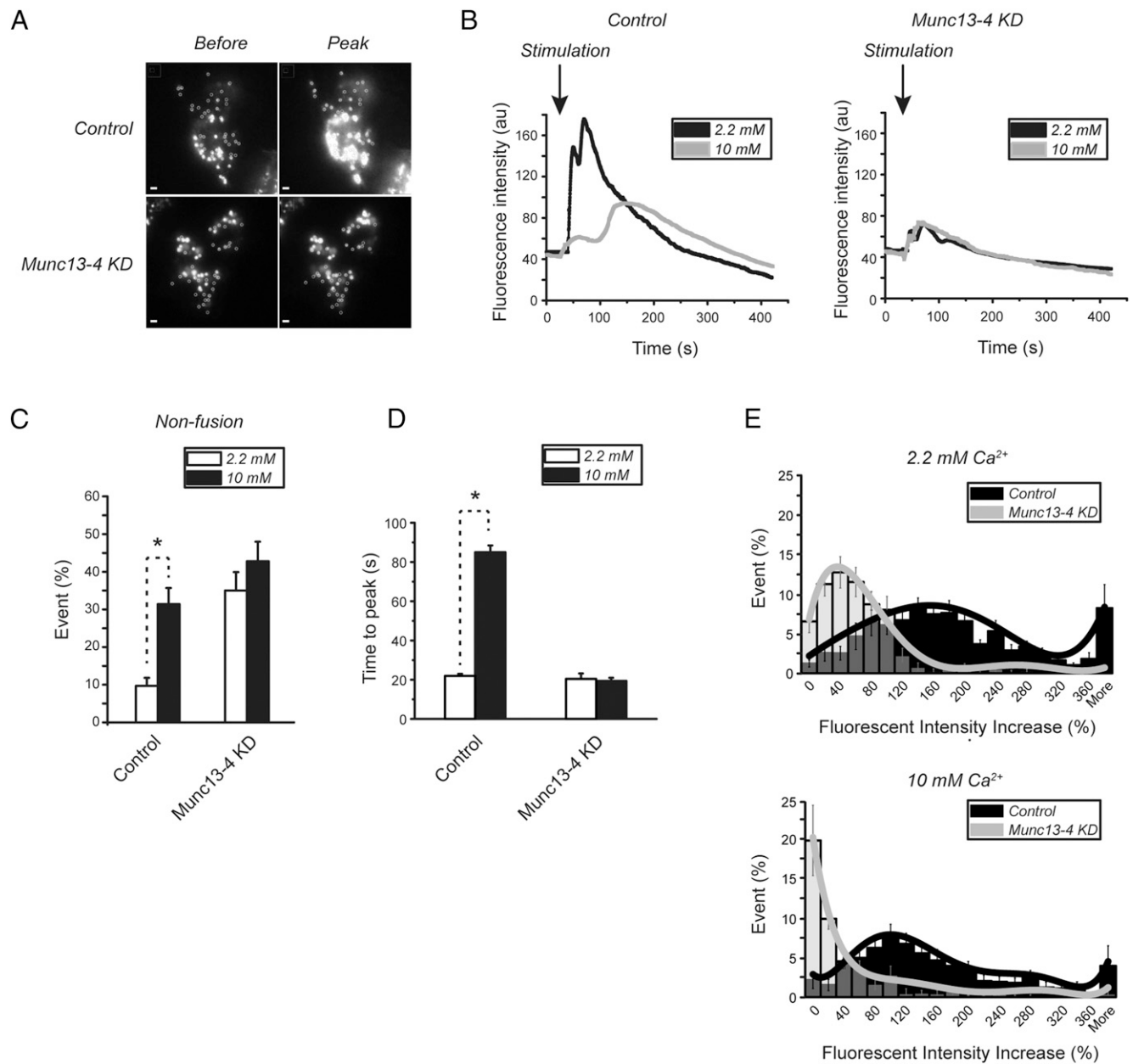
FIGURE 8. Single-granule fusion analysis using TIRFM reveals a role of Munc13-4 in regulating fusion events in a Ca^{2+}-dependent manner. (**A**) Example of NPY-mCherry expressing lysosomal granules in control and Munc13-4 KD cells before stimulation (left) or at the peak of exocytosis (right) under TIRFM. Scale bars, 10 μm. (**B**) Representative trace of release of the NPY-mCherry from single-granule fusions from the control and Munc13-4 KD cells at 2.2 mM (black) and 10 mM (gray) extracellular Ca^{2+}. (**C**) Nonfusion events were calculated by normalizing the number of granules that exhibited nonfusing behavior to the total number of granules in control and Munc13-4 KD cells at 2.2 and 10 mM extracellular Ca^{2+} per cell. Error bars indicate SEM ($n = 15$). (**D**) Kinetic of NPY-mCherry release from fused single granules in each cell was calculated from the time of adding stimulation (2.5 μM ionomycin) to reach the peak of fluorescence intensity at 2.2 and 10 mM extracellular Ca^{2+}. Error bars indicate SEM ($n = 15$). (**E**) Normalized histogram and Gaussian fits illustrating fluorescence intensity increase of single-granule fusion events from control and Munc13-4 KD cells at 2.2 and 10 mM extracellular Ca^{2+}. Percentage of increase was calculated by normalizing peak fluorescence intensity to the baseline of each granule. Error bars indicate SEM ($n = 15$). *$p < 0.05$.

different types of immune cells can fill the gaps of the current study.

Using TIRFM, we unexpectedly found Ca^{2+}-dependent variations in the kinetics and sizes of fusion pore opening as a consequence of Munc13-4 C2 domain mutations (Figs. 8, 9, Supplemental Fig. 4). In neuronal exocytosis, the kinetics of every single-vesicle fusion is believed to be highly uniform. Null mutations of the proteins critical for exocytosis, such as synaptotagmin-1, VAMP2, SNAP-25, and Munc13-1, strikingly reduce the frequency of the fusion events; however, the kinetics

of the remaining fusion events are similar, suggesting that the fusion event is unitary, and the entity that mediates the fusion pore opening remains unclear. However, this unitary nature may be partly attributed to the small size of synaptic vesicles, where the release of a high concentration of transmitters upon the vesicle fusion event would be too rapid. These make it technically difficult to measure the variations in fusion pore opening during synaptic vesicle exocytosis. For example, although two types of synaptic vesicle fusions (kiss-and-run versus full membrane fusion) have been suggested, the measurement of the
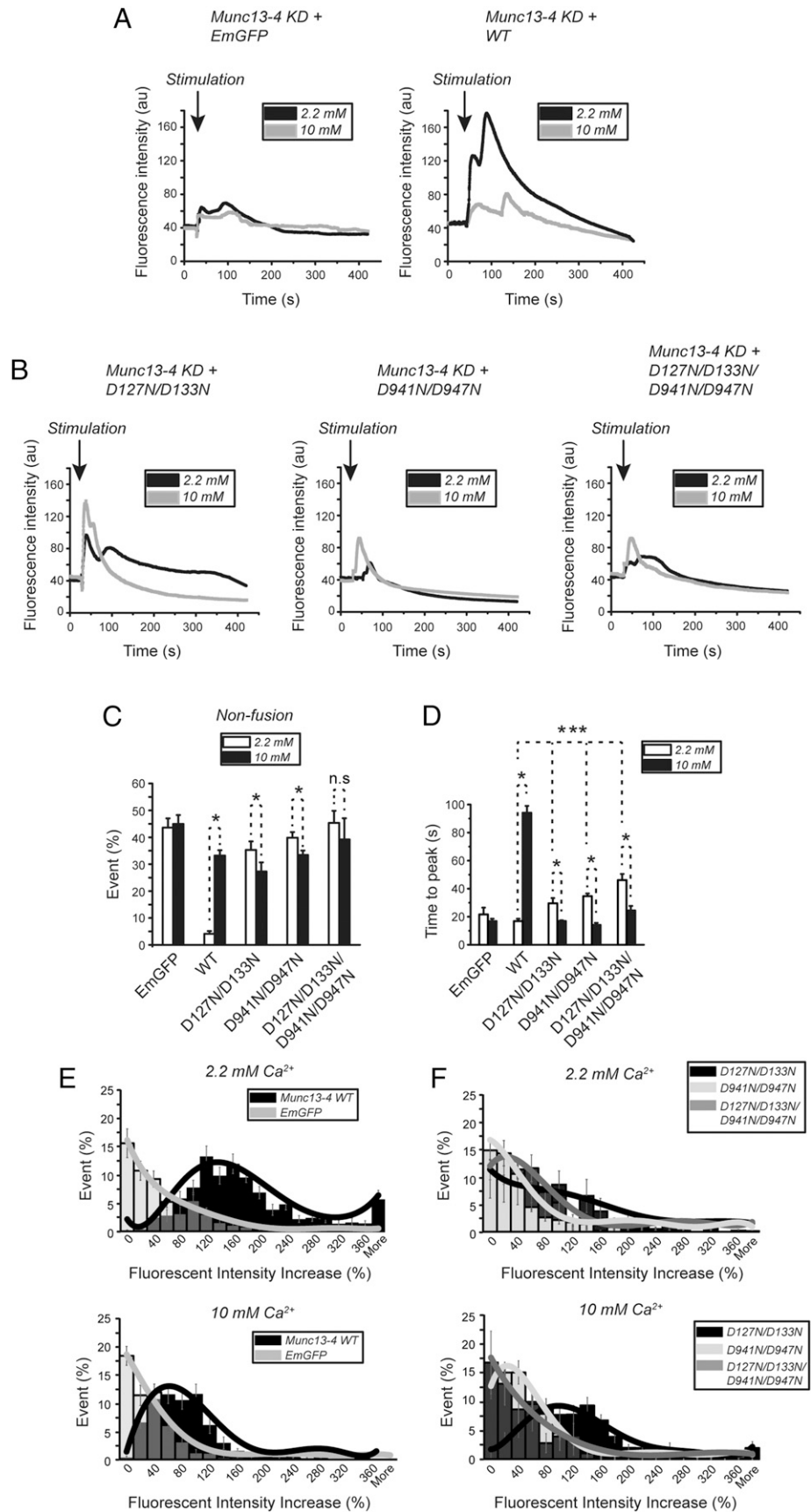
FIGURE 9. Mutations in C2 domains of Munc13-4 strikingly alter the Ca^{2+} sensitivity of single-granule fusion. (**A** and **B**) Representative traces of release of NPY-mCherry from Munc13-4 KD cells rescued with (A) EmGFP, WT, (B) double, and quadruple mutants in C2 domains upon exocytosis triggered at 2.2 mM Ca^{2+} (black) and 10 mM Ca^{2+} (gray). (**C**) Nonfusion events of granules of Munc13-4 KD cells rescued with EmGFP, WT Munc13-4, and double mutants as well as quadruple mutants in C2 domains at 2.2 and 10 mM extracellular Ca^{2+} per cell. $n = 20$ for WT; $n = 14$ for mutants. Error bars indicate SEM. (**D**) Kinetic of NPY-mCherry release from fused single granules in each Munc13-4 KD cell rescued with EmGFP, WT Munc13-4, and double mutants as well as quadruple mutants in C2 domains at 2.2 and 10 mM extracellular Ca^{2+}. $n = 20$ for WT; $n = 14$ for mutants. Error bars indicate SEM. (**E** and **F**) Normalized histogram and Gaussian fits illustrating fluorescence intensity increase of single-granule fusion events from Munc13-4 KD cells rescued with (**E**) EmGFP, WT Munc13-4, and (**F**) double mutants as well as quadruple mutants in C2 domains at 2.2 and 10 mM extracellular Ca^{2+}. Error bars indicate SEM. *$p < 0.05$, ***$p < 0.001$.

kinetics of miniature postsynaptic current does not normally distinguish between these two. Unlike ultrafast neurotransmitter exocytosis, the fusion of large lysosomal vesicles occurs in the order of seconds; thereby, studying fusion pore opening in this system would be more approachable (53–55). In this aspect, further study of the lysosomal vesicle fusion can uniquely

FIGURE 10. Ca^{2+} binding C2 domains and vesicular localization are common for two Ca^{2+} sensors in neuronal and immune cell exocytosis. Top, Two C2 domains of synaptotagmin-1, which localizes to the synaptic vesicles to mediate the Ca^{2+} sensing in neuronal exocytosis. Munc13-1 is localized to the active zone via RIM-binding C2A domain. C2A and C2C domains of Munc13-1 do not bind to Ca^{2+}. Ca^{2+} binding C2B domain, along with calmodulin-binding domain and diacylglycerol-binding C1 domain, is responsible for short-term plasticity (18). MHD mediates an interaction with plasma membrane–localized t-SNARE and syntaxin-1 (59). Bottom, Munc13-4 is localized at secretory lysosomal granules in part via an interaction with Rab27 (7, 20). Two C2 domains of Munc13-4 bind to Ca^{2+} and mediate Ca^{2+} sensing of immune cell exocytosis. MHD of Munc13-4 can potentially interact with syntaxin-3 or -11, both of which are responsible for a priming function of Munc13-4. Synaptotagmin-7, which also localizes to the lysosomal granules, could also be involved in Ca^{2+} sensing (60, 61).
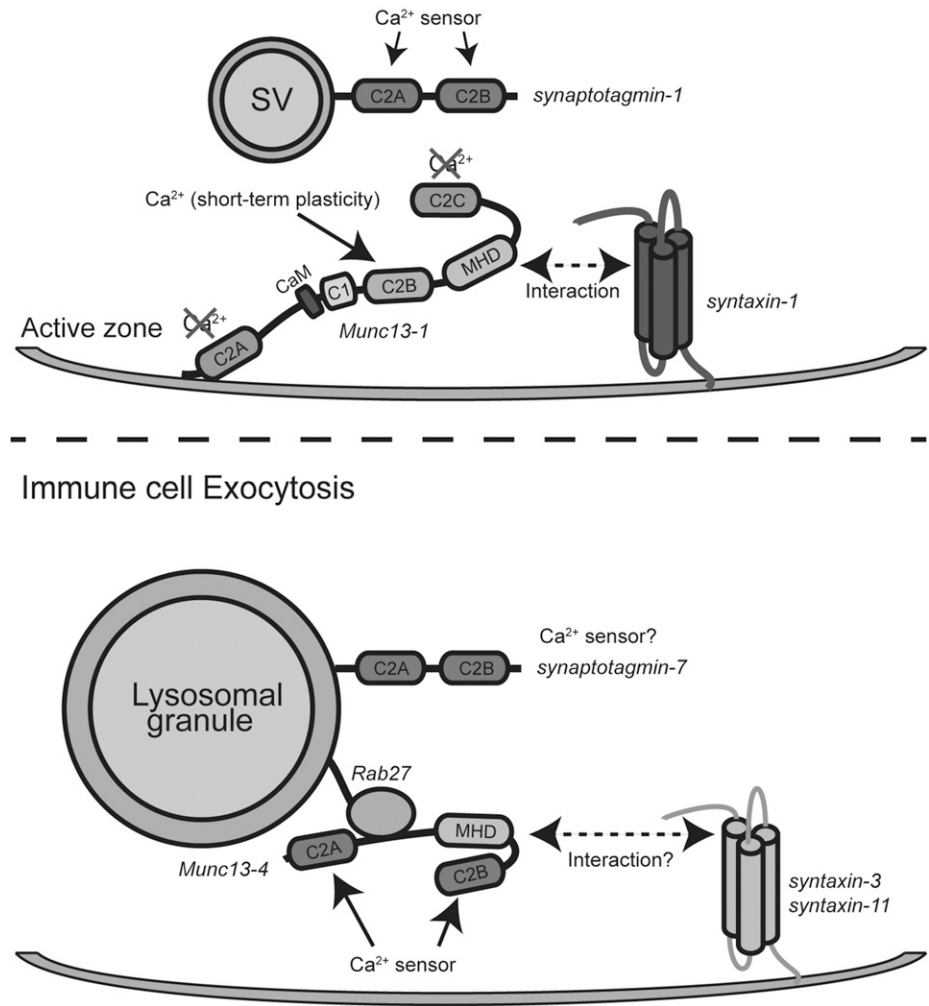
contribute to unraveling mechanisms that regulate the fusion pore opening and closure.

The fact that a devastating immune disorder, FHL3, is implicated by various mutations in Munc13-4 necessitates the understanding of molecular mechanisms in the context of NK cell degranulation (5, 56, 57). Nonetheless, relatively short lifespans of functional primary NK cells in culture as well as the difficulty in genetic manipulation have hindered the performance of such experiments. Indeed, many previous works examining the structural and functional relationship of Munc13-4 have relied on the use of RBL-2H3 cells (7, 58). Using a lentivirus, we have succeeded for the first time, to our knowledge, in expressing human Munc13-4 and fully rescuing exocytosis and cytotoxicity of Munc13-4 KO NK cells (Figs. 3–6). This approach will enable us to continue the study of the structural and functional relationship of Munc13-4 in immune exocytosis as well as to facilitate novel therapeutic interventions against devastating immune diseases.

Disclosures

References

1. Bin, N. R., C. H. Jung, C. Piggott, and S. Sugita. 2013. Crucial role of the hydrophobic pocket region of Munc18 protein in mast cell degranulation. *Proc. Natl. Acad. Sci. USA* 110: 4610–4615.
2. Hong, W. 2005. Cytotoxic T lymphocyte exocytosis: bring on the SNAREs! *Trends Cell Biol.* 15: 644–650.
3. Pattu, V., B. Qu, M. Marshall, U. Becherer, C. Junker, U. Matti, E. C. Schwarz, E. Krause, M. Hoth, and J. Rettig. 2011. Syntaxin7 is required for lytic granule release from cytotoxic T lymphocytes. *Traffic* 12: 890–901.
4. Dressel, R., L. Elsner, P. Novota, N. Kanwar, and G. Fischer von Mollard. 2010. The exocytosis of lytic granules is impaired in Vti1b- or Vamp8-deficient CTL leading to a reduced cytotoxic activity following antigen-specific activation. *J. Immunol.* 185: 1005–1014.
5. Feldmann, J., I. Callebaut, G. Raposo, S. Certain, D. Bacq, C. Dumont, N. Lambert, M. Ouachée-Chardin, G. Chedeville, H. Tamary, et al. 2003. Munc13-4 is essential for cytolytic granules fusion and is mutated in a form of familial hemophagocytic lymphohistiocytosis (FHL3). *Cell* 115: 461–473.
6. Bin, N. R., C. H. Jung, B. Kim, P. Chandrasegram, E. Turlova, D. Zhu, H. Y. Gaisano, H. S. Sun, and S. Sugita. 2015. Chaperoning of closed syntaxin-3 through Lys46 and Glu59 in domain 1 of Munc18 proteins is indispensable for mast cell exocytosis. *J. Cell Sci.* 128: 1946–1960.
7. Elstak, E. D., M. Neeft, N. T. Nehme, J. Voortman, M. Cheung, M. Goodarzifard, H. C. Gerritsen, P. M. van Bergen En Henegouwen, I. Callebaut, G. de Saint Basile, and P. van der Sluijs. 2011. The munc13-4-rab27 complex is specifically required for tethering secretory lysosomes at the plasma membrane. *Blood* 118: 1570–1578.
8. Côte, M., M. M. Ménager, A. Burgess, N. Mahlaoui, C. Picard, C. Schaffner, F. Al-Manjomi, M. Al-Harbi, A. Alangari, F. Le Deist, et al. 2009. Munc18-2 deficiency causes familial hemophagocytic lymphohistiocytosis type 5 and impairs cytotoxic granule exocytosis in patient NK cells. *J. Clin. Invest.* 119: 3765–3773.
9. zur Stadt, U., J. Rohr, W. Seifert, F. Koch, S. Grieve, J. Pagel, J. Strauss, B. Kasper, G. Nürnberg, C. Becker, et al. 2009. Familial hemophagocytic

lymphohistiocytosis type 5 (FHL-5) is caused by mutations in Munc18-2 and impaired binding to syntaxin 11. *Am. J. Hum. Genet.* 85: 482–492.

10. Cetica, V., A. Santoro, K. C. Gilmour, E. Sieni, K. Beutel, D. Pende, S. Marcenaro, F. Koch, S. Grieve, R. Wheeler, et al. 2010. STXBP2 mutations in children with familial haemophagocytic lymphohistiocytosis type 5. *J. Med. Genet.* 47: 595–600.

11. Meeths, M., M. Entesarian, W. Al-Herz, S. C. Chiang, S. M. Wood, W. Al-Ateeqi, F. Almazan, J. J. Boelens, H. Hasle, M. Ifversen, et al. 2010. Spectrum of clinical presentations in familial hemophagocytic lymphohistiocytosis type 5 patients with mutations in STXBP2. *Blood* 116: 2635–2643.

12. Bryceson, Y. T., E. Rudd, C. Zheng, J. Edner, D. Ma, S. M. Wood, A. G. Bechensteen, J. J. Boelens, T. Celkan, R. A. Farah, et al. 2007. Defective cytotoxic lymphocyte degranulation in syntaxin-11 deficient familial hemophagocytic lymphohistiocytosis 4 (FHL4) patients. *Blood* 110: 1906–1915.

13. Barral, D. C., J. S. Ramalho, R. Anders, A. N. Hume, H. J. Knapton, T. Tolmachova, L. M. Collinson, D. Goulding, K. S. Authi, and M. C. Seabra. 2002. Functional redundancy of Rab27 proteins and the pathogenesis of Griscelli syndrome. *J. Clin. Invest.* 110: 247–257.

14. Fernández-Chacón, R., A. Königstorfer, S. H. Gerber, J. García, M. F. Matos, C. F. Stevens, N. Brose, J. Rizo, C. Rosenmund, and T. C. Südhof. 2001. Synaptotagmin I functions as a calcium regulator of release probability. *Nature* 410: 41–49.

15. Geppert, M., Y. Goda, R. E. Hammer, C. Li, T. W. Rosahl, C. F. Stevens, and T. C. Südhof. 1994. Synaptotagmin I: a major Ca2+ sensor for transmitter release at a central synapse. *Cell* 79: 717–727.

16. Brose, N., C. Rosenmund, and J. Rettig. 2000. Regulation of transmitter release by Unc-13 and its homologues. *Curr. Opin. Neurobiol.* 10: 303–311.

17. Augustin, I., A. Betz, C. Herrmann, T. Jo, and N. Brose. 1999. Differential expression of two novel Munc13 proteins in rat brain. *Biochem. J.* 337: 363–371.

18. Shin, O. H., J. Lu, J. S. Rhee, D. R. Tomchick, Z. P. Pang, S. M. Wojcik, M. Camacho-Perez, N. Brose, M. Machius, J. Rizo, et al. 2010. Munc13 C2B domain is an activity-dependent Ca2+ regulator of synaptic exocytosis. *Nat. Struct. Mol. Biol.* 17: 280–288.

19. Boswell, K. L., D. J. James, J. M. Esquibel, S. Bruinsma, R. Shirakawa, H. Horiuchi, and T. F. Martin. 2012. Munc13-4 reconstitutes calcium-dependent SNARE-mediated membrane fusion. *J. Cell Biol.* 197: 301–312.

20. Shirakawa, R., T. Higashi, A. Tabuchi, A. Yoshioka, H. Nishioka, M. Fukuda, T. Kita, and H. Horiuchi. 2004. Munc13-4 is a GTP-Rab27-binding protein regulating dense core granule secretion in platelets. *J. Biol. Chem.* 279: 10730–10737.

21. Crozat, K., K. Hoebe, S. Ugolini, N. A. Hong, E. Janssen, S. Rutschmann, S. Mudd, S. Sovath, E. Vivier, and B. Beutler. 2007. Jinx, an MCMV susceptibility phenotype caused by disruption of Unc13d: a mouse model of type 3 familial hemophagocytic lymphohistiocytosis. [Published erratum appears in 2008 *J. Exp. Med.* 205: 737.] *J. Exp. Med.* 204: 853–863.

22. Hsu, P. D., D. A. Scott, J. A. Weinstein, F. A. Ran, S. Konermann, V. Agarwala, Y. Li, E. J. Fine, X. Wu, O. Shalem, et al. 2013. DNA targeting specificity of RNA-guided Cas9 nucleases. *Nat. Biotechnol.* 31: 827–832.

23. Matsuda, T., and C. L. Cepko. 2007. Controlled expression of transgenes introduced by in vivo electroporation. *Proc. Natl. Acad. Sci. USA* 104: 1027–1032.

24. Baumlin-Schmid, N., M. Salathe, and N. L. Fregien. 2016. Optimal lentivirus production and cell culture conditions necessary to successfully transduce primary human bronchial epithelial cells. *J. Vis. Exp.* 113: e54176. Available at: https://www.jove.com/video/54176/optimal-lentivirus-production-cell-culture-conditions-necessary-to.

25. Alter, G., J. M. Malenfant, and M. Altfeld. 2004. CD107a as a functional marker for the identification of natural killer cell activity. *J. Immunol. Methods* 294: 15–22.

26. Neri, S., E. Mariani, A. Meneghetti, L. Cattini, and A. Facchini. 2001. Calcein-acetyoxymethyl cytotoxicity assay: standardization of a method allowing additional analyses on recovered effector cells and supernatants. *Clin. Diagn. Lab. Immunol.* 8: 1131–1135.

27. Xie, L., D. Zhu, Y. Kang, T. Liang, Y. He, and H. Y. Gaisano. 2013. Exocyst sec5 regulates exocytosis of newcomer insulin granules underlying biphasic insulin secretion. *PLoS One* 8: e67561.

28. Cheng, Y., S. M. Sequeira, L. Malinina, V. Tereshko, T. H. Söllner, and D. J. Patel. 2004. Crystallographic identification of Ca2+ and Sr2+ coordination sites in synaptotagmin I C2B domain. *Protein Sci.* 13: 2665–2672.

29. Biasini, M., S. Bienert, A. Waterhouse, K. Arnold, G. Studer, T. Schmidt, F. Kiefer, T. Gallo Cassarino, M. Bertoni, L. Bordoli, and T. Schwede. 2014. SWISS-MODEL: modelling protein tertiary and quaternary structure using evolutionary information. *Nucleic Acids Res.* 42: W252–W258.

30. Arnold, K., L. Bordoli, J. Kopp, and T. Schwede. 2006. The SWISS-MODEL workspace: a web-based environment for protein structure homology modelling. *Bioinformatics* 22: 195–201.

31. Kiefer, F., K. Arnold, M. Künzli, L. Bordoli, and T. Schwede. 2009. The SWISS-MODEL repository and associated resources. *Nucleic Acids Res.* 37: D387–D392.

32. Guex, N., M. C. Peitsch, and T. Schwede. 2009. Automated comparative protein structure modeling with SWISS-MODEL and Swiss-PdbViewer: a historical perspective. *Electrophoresis* 30(Suppl. 1): S162–S173.

33. Tadokoro, S., T. Kurimoto, M. Nakanishi, and N. Hirashima. 2007. Munc18-2 regulates exocytotic membrane fusion positively interacting with syntaxin-3 in RBL-2H3 cells. *Mol. Immunol.* 44: 3427–3433.

34. Brochetta, C., R. Suzuki, F. Vita, M. R. Soranzo, J. Claver, L. C. Madjene, T. Attout, J. Vitte, N. Varin-Blank, G. Zabucchi, et al. 2014. Munc18-2 and syntaxin 3 control distinct essential steps in mast cell degranulation. *J. Immunol.* 192: 41–51.

35. Jung, I. D., H. S. Lee, H. Y. Lee, and O. H. Choi. 2009. FcepsilonRI-mediated mast cell migration: signaling pathways and dependence on cytosolic free Ca2+ concentration. *Cell. Signal.* 21: 1698–1705.

36. Ryu, S. D., H. S. Lee, H. Y. Suk, C. S. Park, and O. H. Choi. 2009. Cross-linking of FcepsilonRI causes Ca2+ mobilization via a sphingosine kinase pathway in a clathrin-dependent manner. *Cell Calcium* 45: 99–108.

37. Zhang, K., A. H. Filipovich, J. Johnson, R. A. Marsh, and J. Villanueva. 1993. Hemophagocytic Lymphohistiocytosis, Familial. In GeneReviews. M. P. Adam, H. H. Ardinger, R. A. Pagon, S. E. Wallace, L. J. H. Bean, K. Stephens, and A. Amemiya, eds. University of Washington, Seattle, WA. Available at: https://www.ncbi.nlm.nih.gov/books/NBK1444/. Accessed: June 1, 2018.

38. Giorda, R., E. P. Weisberg, T. K. Ip, and M. Trucco. 1992. Genomic structure and strain-specific expression of the natural killer cell receptor NKR-P1. *J. Immunol.* 149: 1957–1963.

39. Savan, R., T. Chan, and H. A. Young. 2010. Lentiviral gene transduction in human and mouse NK cell lines. *Methods Mol. Biol.* 612: 209–221.

40. Wang, H., H. Yang, C. S. Shivalila, M. M. Dawlaty, A. W. Cheng, F. Zhang, and R. Jaenisch. 2013. One-step generation of mice carrying mutations in multiple genes by CRISPR/Cas-mediated genome engineering. *Cell* 153: 910–918.

41. Yang, H., H. Wang, C. S. Shivalila, A. W. Cheng, L. Shi, and R. Jaenisch. 2013. One-step generation of mice carrying reporter and conditional alleles by CRISPR/Cas-mediated genome engineering. *Cell* 154: 1370–1379.

42. Varoqueaux, F., A. Sigler, J. S. Rhee, N. Brose, C. Enk, K. Reim, and C. Rosenmund. 2002. Total arrest of spontaneous and evoked synaptic transmission but normal synaptogenesis in the absence of Munc13-mediated vesicle priming. *Proc. Natl. Acad. Sci. USA* 99: 9037–9042.

43. Pivot-Pajot, C., F. Varoqueaux, G. de Saint Basile, and S. G. Bourgoin. 2008. Munc13-4 regulates granule secretion in human neutrophils. *J. Immunol.* 180: 6786–6797.

44. Yamaga, M., D. M. Kielar-Grevstad, and T. F. Martin. 2015. Phospholipase Cη2 activation redirects vesicle trafficking by regulating F-actin. *J. Biol. Chem.* 290: 29010–29021.

45. Shin, O. H., J. Xu, J. Rizo, and T. C. Südhof. 2009. Differential but convergent functions of Ca2+ binding to synaptotagmin-1 C2 domains mediate neurotransmitter release. *Proc. Natl. Acad. Sci. USA* 106: 16469–16474.

46. Chicka, M. C., Q. Ren, D. Richards, L. M. Hellman, J. Zhang, M. G. Fried, and S. W. Whiteheart. 2016. Role of Munc13-4 as a Ca2+-dependent tether during platelet secretion. *Biochem. J.* 473: 627–639.

47. Sutton, R. B., B. A. Davletov, A. M. Berghuis, T. C. Südhof, and S. R. Sprang. 1995. Structure of the first C2 domain of synaptotagmin I: a novel Ca2+/phospholipid-binding fold. *Cell* 80: 929–938.

48. Topham, N. J., and E. W. Hewitt. 2009. Natural killer cell cytotoxicity: how do they pull the trigger? *Immunology* 128: 7–15.

49. Woska, J. R., Jr., and M. E. Gillespie. 2012. SNARE complex-mediated degranulation in mast cells. *J. Cell. Mol. Med.* 16: 649–656.

50. Rodarte, E. M., M. A. Ramos, A. J. Davalos, D. C. Moreira, D. S. Moreno, E. I. Cardenas, A. I. Rodarte, Y. Petrova, S. Molina, L. E. Rendon, et al. 2018. Munc13 proteins control regulated exocytosis in mast cells. *J. Biol. Chem.* 293: 345–358.

51. Marcenaro, S., F. Gallo, S. Martini, A. Santoro, G. M. Griffiths, M. Aricó, L. Moretta, and D. Pende. 2006. Analysis of natural killer-cell function in familial hemophagocytic lymphohistiocytosis (FHL): defective CD107a surface expression heralds Munc13-4 defect and discriminates between genetic subtypes of the disease. *Blood* 108: 2316–2323.

52. Wood, S. M., M. Meeths, S. C. Chiang, A. G. Bechensteen, J. J. Boelens, C. Heilmann, H. Horiuchi, S. Rosthøj, O. Rutynowska, J. Winiarski, et al. 2009. Different NK cell-activating receptors preferentially recruit Rab27a or Munc13-4 to perforin-containing granules for cytotoxicity. *Blood* 114: 4117–4127.

53. Fernández-Chacón, R., and G. Alvarez de Toledo. 1995. Cytosolic calcium facilitates release of secretory products after exocytotic vesicle fusion. *FEBS Lett.* 363: 221–225.

54. Oberhauser, A. F., and J. M. Fernandez. 1996. A fusion pore phenotype in mast cells of the ruby-eye mouse. *Proc. Natl. Acad. Sci. USA* 93: 14349–14354.

55. Spruce, A. E., L. J. Breckenridge, A. K. Lee, and W. Almers. 1990. Properties of the fusion pore that forms during exocytosis of a mast cell secretory vesicle. *Neuron* 4: 643–654.

56. Yamamoto, K., E. Ishii, M. Sako, S. Ohga, K. Furuno, N. Suzuki, I. Ueda, M. Imayoshi, S. Yamamoto, A. Morimoto, et al. 2004. Identification of novel MUNC13-4 mutations in familial haemophagocytic lymphohistiocytosis and functional analysis of MUNC13-4-deficient cytotoxic T lymphocytes. *J. Med. Genet.* 41: 763–767.

57. Santoro, A., S. Cannella, G. Bossi, F. Gallo, A. Trizzino, D. Pende, F. Dieli, G. Bruno, J. C. Stinchcombe, C. Micalizzi, et al. 2006. Novel Munc13-4 mutations in children and young adult patients with haemophagocytic lymphohistiocytosis. *J. Med. Genet.* 43: 953–960.

58. Neeft, M., M. Wieffer, A. S. de Jong, G. Negroiu, C. H. Metz, A. van Loon, J. Griffith, J. Krijgsveld, N. Wulffraat, H. Koch, et al. 2005. Munc13-4 is an effector of rab27a and controls secretion of lysosomes in hematopoietic cells. *Mol. Biol. Cell* 16: 731–741.

59. Betz, A., M. Okamoto, F. Benseler, and N. Brose. 1997. Direct interaction of the rat unc-13 homologue Munc13-1 with the N terminus of syntaxin. *J. Biol. Chem.* 272: 2520–2526.

60. Chakrabarti, S., K. S. Kobayashi, R. A. Flavell, C. B. Marks, K. Miyake, D. R. Liston, K. T. Fowler, F. S. Gorelick, and N. W. Andrews. 2003. Impaired membrane resealing and autoimmune myositis in synaptotagmin VII–deficient mice. *J. Cell Biol.* 162: 543–549.

61. Martinez, I., S. Chakrabarti, T. Hellevik, J. Morehead, K. Fowler, and N. W. Andrews. 2000. Synaptotagmin VII regulates Ca(2+)-dependent exocytosis of lysosomes in fibroblasts. *J. Cell Biol.* 148: 1141–1149.